CHEMISTRY OF MATERIALS

Article

pubs.acs.org/cm

Mesoporous Silica Supported Au and AuCu Nanoparticles for Surface Plasmon Driven Glycerol Oxidation

Stefan Schünemann, Georgios Dodekatos, and Harun Tüysüz*

Max-Planck-Institut für Kohlenforschung, 45470 Mülheim an der Ruhr, Germany

Supporting Information

ABSTRACT: Herein, we report for the first time the visible-light-assisted rate enhancement for glycerol oxidation using direct plasmonic photocatalysis. Au nanoparticles were loaded on various mesoporous SiO_2 supports, and the catalytic performance was investigated with and without visible-light illumination. Monodispersed mesoporous silica spheres loaded with Au nanoparticles demonstrated a superior photoassisted catalytic rate enhancement compared to Au loaded ordered mesoporous silica (SBA-15, KIT-6, and MCM-41). The enhancement is attributed to the particle size of the Au nanoparticles and better light interaction resulting from the small SiO_2 domains. Au loaded monodispersed mesoporous silica spheres exhibit a constant and remarkably small particle diameter of 2 nm at Au loadings of up to 15 wt % as a result of the support's small domain size and efficient pore confinement. The performance of the Au catalyst could be further improved by preparing bimetallic AuCu nanoparticles. Synergistic effects between Au and Cu improved the glycerol conversion by a factor of 2.5 and the dihydroxyacetone selectivity from 80% to 90% compared to monometallic Au catalysts.

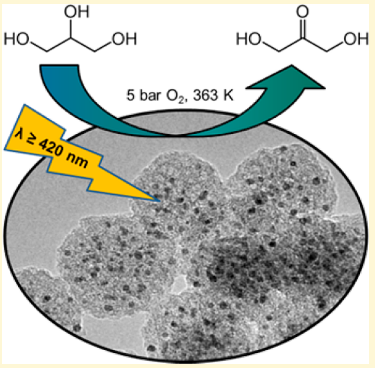

INTRODUCTION

The rapidly growing global population, environmental concerns, and upcoming shortages in fossil fuels have resulted in considerable interest for alternative energy sources. In this regard, biodiesel production has increased during the past few decades and is utilized as a green energy fuel. The production of biodiesel results in a higher supply of glycerol (10 wt % of the biodiesel),[1] which is largely treated as waste material.[2,3] In this regard the selective oxidation of glycerol plays among dehydration,[4] esterification[3,5] and hydrogenolysis[6] an important role. Many reports have emerged for the selective oxidation of glycerol by using various metal particles immobilized on different supports.[7−10] Prati and Rossi were the first to demonstrate that supported Au nanoparticles (NPs) are capable of alcohol oxidation.[11] The catalytic activity and selectivity of Au catalysts for selective oxidation reactions can be increased by alloying of Au with various metals such as Pd, Pt, and Cu due to synergistic effects between both metals.[12,13]

Aside from using noble metal NPs in conventional heat driven catalysis for organic transformation reactions, their use in plasmonic photocatalysis is a strongly emerging field for driving these reactions with the aid of (preferentially visible) light. In conventional photocatalysis, photons provided by a light source, which is in the ideal case the sun, are utilized to drive chemical reactions on heterogeneous interfaces. The typical drawbacks are poor visible-light harvesting and low quantum efficiencies; that is, generated charge carriers in the semiconductor are mainly dissipated as heat as a result of charge carrier recombination.[14,15] Plasmonic photocatalysis with metal NPs provides a great opportunity to overcome these disadvantages. In particular, direct plasmonic photocatalysis (DPP) is an appealing integrated system where plasmonic NPs act as both visible-light absorber and active site for the chemical reaction.[16,17] The application of conventional photocatalysis in selective oxidation reactions often suffers from low selectivity due to the high oxidation potentials of most semiconductors, a problem which is completely avoided in DPP.[18,19] An inherent benefit of DPP is the broader choice of applicable supports, as there is no limitation to light absorbing semiconductors, as in conventional plasmonic photocatalysis. This allows the application of supports with desirable properties such as efficient pore confinement of metal NPs, high surface area, facile morphology control, abundance and cost efficiency.

In DPP, light with a suitable wavelength interacts with a metal plasmonic NP and the oscillating electromagnetic field causes coherent oscillations of the conduction band electrons of the metal NP, so-called localized surface plasmon resonance (LSPR).[16] The decay of surface plasmons proceeds via three pathways, a radiative (i.e., scattering) and two nonradiative pathways, namely, Landau damping and chemical interface damping. In both nonradiative damping mechanisms, electrons are transferred from the plasmonic NP to an unoccupied molecular orbital in adsorbed molecules which, after back-transfer of the electron, leave the adsorbate in a vibrationally excited state. Thus, DPP reduces the activation barrier of certain elementary steps, which accelerates kinetics and opens reaction pathways that are not achievable with thermal energy

Received: September 9, 2015
Revised: October 21, 2015
Published: October 27, 2015

DOI: 10.1021/acs.chemmater.5b03520
Chem. Mater. 2015, 27, 7743−7750

alone to manipulate selectivities.[17] Linic et al. showed that this charge carrier injection into the lowest unoccupied molecular orbital of molecularly adsorbed O_2 on Ag NPs reduces the activation energy for its dissociation.[16] The selective oxidation of alcohols via DPP with supported Au NPs previously showed superior photocatalytic activity compared to the solely thermal reaction.[20,21] The (photo-)catalytic activity and selectivity of Au catalysts in selective oxidation reactions can also be increased by alloying of Au with various metals such as Pd, Pt, and Cu due to synergistic effects between both metals.[13,22,23] Hirai et al. showed that TiO_2 supported AuCu alloy NPs show an increased activity under visible-light irradiation for the selective oxidation of 2-propanol to acetone due to efficient O_2 activation at alloy sites.[24]

High surface area mesoporous materials provide an excellent platform for the deposition of active components, mainly due to their pore confinement. On the other hand, morphology, domain size, and the pore system of the support can play a significant role for deposition of uniform active components as well. The recently reported monodispersed mesoporous silica spheres[25] with a mean diameter of 40 nm and with spherical pores with a mean diameter of 2.3 nm could supply an exceptional platform for deposition of very small nanoparticles. This morphology is thought to facilitate the homogeneous infiltration of the metal precursor due to the small and controllable domain size and the cage-like pores, which confine metal NPs more efficiently than tubular pores of ordered mesoporous silica materials such as SBA-15 and MCM-41.[26,27]

Despite its commercial value, only a few reports have been published for photocatalytic reactions involving glycerol,[28−30] and to the best of our knowledge, there are no reports utilizing DPP for the oxidation of glycerol. To demonstrate the importance of the nature of the support, herein, we design a series of mesoporous silica supported Au and AuCu nanoparticles for surface plasmon driven glycerol oxidation. Mesoporous silica spheres loaded with Au nanoparticles indicated higher photoassisted catalytic activity in comparison with Au loaded ordered mesoporous silica (SBA-15, KIT-6, and MCM-41). The improvement is ascribed to the particle size of the Au nanoparticles and better light interaction resulting from the small domain size of mesoporous silica spheres. All of the catalysts showed higher glycerol conversions under visible-light illumination. This surface plasmon driven catalysis could be an alternative method for traditional heterogeneous catalysis.

EXPERIMENTAL SECTION

All chemicals were used as purchased without further purification. The following chemicals were purchased from Sigma-Aldrich: cetyltrimethylammonium bromide (CTAB; ≥99.0%), triethanolamine (≥99%), tetraethyl orthosilicate (TEOS, 98%), (3-aminopropyl)-trimethoxysilane (APS; 97%), Pluronic P123 (average $M_n \sim 5{,}800$), NH_4OH (28.0−30.0% NH_3 basis), chloroauric acid trihydrate (≥49% Au basis), and copper(II) nitrate trihydrate (99−104%). Ethylenediamine (en) was purchased from Fluka (≥99.5%). *n*-Butanol was purchased from Merck (≥99.8%). NaOH was purchased from VWR. HCl (37%) was purchased from J. T. Baker.

Monodispersed Mesoporous Silica Spheres. Monodispersed mesoporous silica nanospheres (MSs) were synthesized via soft templating according to a literature procedure.[31] A 7.675 g (21 mmol) amount of CTAB was dissolved in 500 mL of deionized (DI) water in a polypropylene bottle. The suspension was stirred for 5 min and subsequently sonicated for 20 min. Afterward, the solution was placed in an oven at 100 °C for 10 min to completely dissolve CTAB. A 1.545 mL aliquot (11.6 mmol) of triethanolamine was added, and the solution was stirred at 80 °C for 1 h. Then 77.55 mL (347 mmol) of TEOS was rapidly added to the stirring solution which was subsequently stirred at 80 °C for 2 h. The cold suspension was centrifuged (11000 min^{-1}, 45 min.) and subsequently placed in an oven to dry (90 °C, 16 h). The dried powder was calcined at 550 °C for 6 h. The obtained monodispersed mesoporous silica spheres are designated as MS.

(3-Aminopropyl)trimethoxysilane Surface Functionalized Monodispersed Mesoporous Silica Spheres.[32] A 1 g amount of as prepared MS was added to a solution of 10 mL of APS and 10 mL of DI water. The suspension was stirred overnight, followed by centrifugation (9000 min^{-1}, 20 min) and decantation of the excess solvent and resuspending the silica material in DI water under sonication. This process was repeated twice to obtain surface modified monodispersed mesoporous silica spheres (MS-APS).

Preparation of KIT-6 Silica.[33] A 13.5 g amount of Pluronic P123 was dissolved in a mixture of 487.5 g of DI water and 26.1 g of HCl (37%) and stirred for 1 h. Then 13.5 g of *n*-butanol was added at a temperature of 35 °C followed by 1 h of stirring at this temperature. Subsequently, 29 g of TEOS was quickly added and the mixture was stirred for 24 h at 35 °C. Afterward, hydrothermal treatment was carried out at 100 °C for 24 h. The white powder was collected by suction filtration, dried overnight at 90 °C, and subsequently calcined for 6 h at 550 °C.

Preparation of SBA-15 Silica.[34] The synthesis of SBA-15 is very similar to that of KIT-6 except that no *n*-butanol is needed. Briefly, 13.9 g of P123 was added to a mixture of 252 g of DI water and 7.75 g of HCl (37%). The mixture was stirred for 1 h until a homogeneous solution was obtained. The solution was heated to 35 °C, and 29.96 g of TEOS was quickly added. The mixture was stirred at 35 °C for 24 h, followed by hydrothermal treatment for 24 h at 100 °C. The white powder was collected by filtration, dried overnight at 90 °C, and subsequently calcined for 6 h at 550 °C.

Preparation of MCM-41 Silica.[35] Unlike KIT-6 and SBA-15, MCM-41 is synthesized under basic conditions. A 1 g amount of CTAB is dissolved in a solution of 156.4 g of DI water and 81.2 mL of NH_4OH. The mixture was stirred until a clear solution was obtained to which 5 mL of TEOS was rapidly added. The mixture was stirred for 2 h, and the white powder was obtained by filtration and washing with DI water. The powder was dried overnight at 50 °C and subsequently calcined for 6 h at 550 °C.

Au Deposition on Silica Supports.[36] To deposit gold on the SiO_2 surface, the cationic complex $[Au(en)_2]Cl_3$ has to be synthesized first. To do so, 800 mg of chloroauric acid trihydrate (2.0 mmol) is dissolved in 8 mL of DI water. In the following, 325 mg of ethylenediamine (en; 5.4 mmol) is added to the stirring solution under exclusion of light. The mixture was stirred for 30 min before 54 mL of ethanol was added followed by stirring for an additional 30 min. The yellow precipitate was collected by vacuum filtration and washed with excess ethanol. The powder was dried overnight at 50 °C under vacuum. To deposit gold nanoparticles on the SiO_2 surface, in a typical synthesis 500 mg of the SiO_2 support was suspended in 38 mL of DI water. The pH of the suspension was adjusted to 10 by a 5 wt % NaOH solution. Then, the required amount of $[Au(en)_2]Cl_3$ was added under vigorous stirring into the darkened solution. The pH was again adjusted to 10 by adding 5 wt% NaOH solution. The mixture was stirred at room temperature for at least 2 h. Afterward, the suspension was cleaned by centrifugation (9 k min^{-1}, 20 min) followed by decantation of the excess solvent and resuspending the silica material in water under sonication. This process was repeated twice. The solid was then collected and dried overnight at 50 °C in vacuo. To reduce Au^{III} to form gold NPs, the yellow powders were reduced under flowing hydrogen at a temperature of 200 °C for 2 h with a temperature ramp of 5 °C min^{-1}. After reduction dark red powders were obtained. Gold deposited on mesoporous silica spheres is designated as *X*−*Y* with *X* indicating the gold loading in weight percent and *Y* indicating the type of support used (MS, KIT-6, SBA-15, or MCM-41).

Au and Cu Deposition on MS-APS. A series of bimetallic Au/Cu loaded MS-APS were synthesized by adding the required amounts of $HAuCl_4 \cdot 3H_2O$, $Cu(NO_3)_2 \cdot 3H_2O$, and 180 mg of urea (3.0 mmol) to a

DOI: 10.1021/acs.chemmater.5b03520
Chem. Mater. 2015, 27, 7743−7750

suspension of MS-APS. The suspension was stirred at 80 °C for 4 h followed by centrifugation and decantation of the excess solvent and resuspending the silica material in water under sonication. This process was repeated twice. The solid was then collected and dried overnight at 50 °C in vacuo. Subsequently, the samples were reduced in flowing H_2 for 2 h at 200 °C with a temperature ramp of 5 °C min^{-1}. The samples are denoted as *X*/*Y*-MS-APS with *X* and *Y* representing the nominal loading of Au and Cu in weight percent, respectively.

Characterization. TEM micrographs were recorded with a Hitachi H-7100 electron microscope with an acceleration voltage of 100 kV. High resolution TEM micrographs and spot-EDX measurements were conducted with a Hitachi HF-2000 field emission electron microscope and an acceleration voltage of 200 kV. STEM micrographs in secondary electron and z-contrast, and elemental mapping of Au and Cu via the AuL and CuK lines, were recorded with a Hitachi HD-2700 field emission scanning transmission electron microscope (FE-STEM) with an acceleration voltage of 200 kV. EDX data were obtained from a Hitachi S-3500N microscope. DR-UV−vis spectra of powdered samples were recorded from 800 to 200 nm with a Varian Cary 5G UV−vis−near-IR spectrophotometer equipped with a Harrick praying-mantis sample holder. MgO NPs from Sigma-Aldrich were used to record the baseline. X-ray photoelectron spectra were recorded with a Kratos His spectrometer equipped with a spherical analyzer. Nitrogen physisorption isotherms were measured at liquid nitrogen temperature with a NOVA 3200e. All samples were degassed at 120 °C for 19 h prior to the measurement. The surface area was determined from multipoint BET method at relative pressures from 0.06 to 0.2. The pore size distribution was determined with the BJH algorithm from the desorption isotherm. The total pore volume was determined at a relative pressure of 0.97.

Catalytic Test: Glycerol Oxidation. Glycerol oxidation was carried out in a sealed autoclave equipped with a borosilicate glass window for illumination. The glass inlay of the autoclave was equipped with 5 mL of a 0.05 M aqueous glycerol solution, 5 mg of catalyst, and a magnetic stirring bar. The suspension was sonicated for 2 min. The photoassisted and thermal reactions were conducted under identical conditions. Prior to heating, the sealed autoclaves were flushed with pure oxygen for 2 min and then loaded with 5 bar pure oxygen at room temperature. In a standard experiment, the autoclaves were heated from room temperature to 90 °C within 30 min and kept at this temperature for a further 4.5 h to give a total reaction time of 5 h. The autoclave was illuminated with a 300 W Xe arc lamp equipped with a Newport long-pass filter with a 420 nm cutoff wavelength (Newport 20CGA-420) and a water filter to cut off IR fractions of the light source. The incident light intensity is 795 mW/cm^2 in the interval from 400 to 800 nm (determined via an Avantes AvaSpec-3648 spectroradiometer). After the reaction, the autoclaves were immediately cooled in an ice bath and the reaction mixtures were centrifuged (14.5 k min^{-1}, 30 min) to separate the solid catalyst from the reaction solution. Since volume changes during the reaction were observed, the conversions and selectivities were calculated from the final volume. The liquid was analyzed via HPLC with a 300 mm organic acid resin with 8.0 mm in diameter with 10 mmol of trifluoroacetic acid and 10 μm of sample. Reaction products were detected at a wavelength of 270 nm. DHA was detected from the solution's refractive index. Detailed calculations for the glycerol conversion, selectivity, carbon balance, and errors can be found in the Supporting Information.

RESULTS AND DISCUSSION

In this study, we prepared and characterized Au and bimetallic AuCu NPs immobilized on silica supports and evaluated the photocatalytic rate enhancement for selective glycerol oxidation under visible-light illumination in neutral pH conditions. In order to study the effect of the support, first different silica supports, such as MSs with a mean diameter of 40 nm and diverse ordered mesoporous silica (om-SiO_2) materials, namely, KIT-6, SBA-15, and MCM-41, were synthesized in a large scale. MS was chosen as a support since the small domain size can allow for the homogeneous deposition of Au throughout the entire support. In addition, the small domain size of the support reduces light scattering and thus allows for a more efficient interaction between the Au NPs and the incident light.[37] Initially, the synthesized silica supports were decorated with 6 wt % Au via cation adsorption of $[Au(en)_2]Cl_3$ in alkaline media and subsequent reduction in H_2.[38] In the following, the samples are denoted as *X*−*Y*, where *X* represents the nominal amount of Au in weight percent, confirmed by EDX measurements (Supporting Information Table S1) and *Y* indicates the type of support.

Due to the large domains of om-SiO_2, Au deposition on these supports resulted in inhomogeneous distribution with Au enrichment on the external surface and, consequently, large mean Au particle diameters. A detailed transmission electron microscopy (TEM) survey (Supporting Information Figure S1) indicated that the mean particle sizes of the Au on KIT-6, SBA-15, and MCM-41 were around 4, 6, and 11 nm, respectively (with standard deviations of about 4 nm). In particular, the small pore size of MCM-41 limits homogeneous impregnation, distribution, and formation of small Au nanoparticles. In contrast, the small domains of MS result in a homogeneous infiltration of the Au precursor and consequently to the formation of small Au particles with a mean diameter of 2 nm. This shows that the nature of the support has a great influence on the size of the plasmonic particles. Since the plasmonic NPs in DPP act as both light absorber and catalytic active sites, the particle size, and consequently the nature of the SiO_2 support, will greatly affect the photocatalytic activity.[39] Small particles provide a large surface area but only weakly absorb visible light at diameters smaller than 2 nm due to quantum confinement.[40] In contrast, large plasmonic particles strongly absorb visible light due to LSPR but only provide a relatively small catalytically active surface area.

The catalytic performance of the 6 wt % Au loaded mesoporous silica for glycerol oxidation under dark and light illumination are presented in Figure 1. As seen in Figure 1, all Au loaded samples showed higher conversion under visible-light illumination (by plasmon driven catalysis) compared to without light. However, in the case of the visible-light driven reaction conditions MS loaded with gold showed, compared to the ordered mesoporous supports, much better efficiency, which confirms that the nature of the support for plasmonic

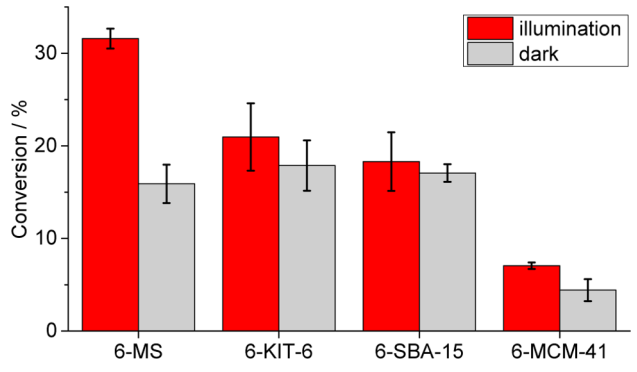

Figure 1. Glycerol conversion under visible-light illumination (red bars) and dark conditions (gray bars): 5 mL of 0.05 M aqueous glycerol solution, neutral pH, 90 °C, 5 mg of photocatalyst, and 5 h reaction time. Light source is 300 W Xe arc lamp equipped with a 420 nm cutoff filter and an IR water filter.

DOI: 10.1021/acs.chemmater.5b03520
Chem. Mater. 2015, 27, 7743−7750

catalysis plays an important role. For Au loaded MS, the glycerol conversion was doubled under light illumination. Au loading of MS resulted in small Au particles with a mean diameter of 2 ± 0.3 nm, which are among the smallest SiO_2 supported Au particles reported in literature (TEM image, Supporting Information Figure S2c).[41] These, compared to most Au/SiO_2 materials reported in literature, exceptionally small Au particles provide an extraordinarily large Au surface area while still allowing visible-light absorption by LSPR as shown by diffuse reflectance UV−vis spectroscopy (Figure 2e).

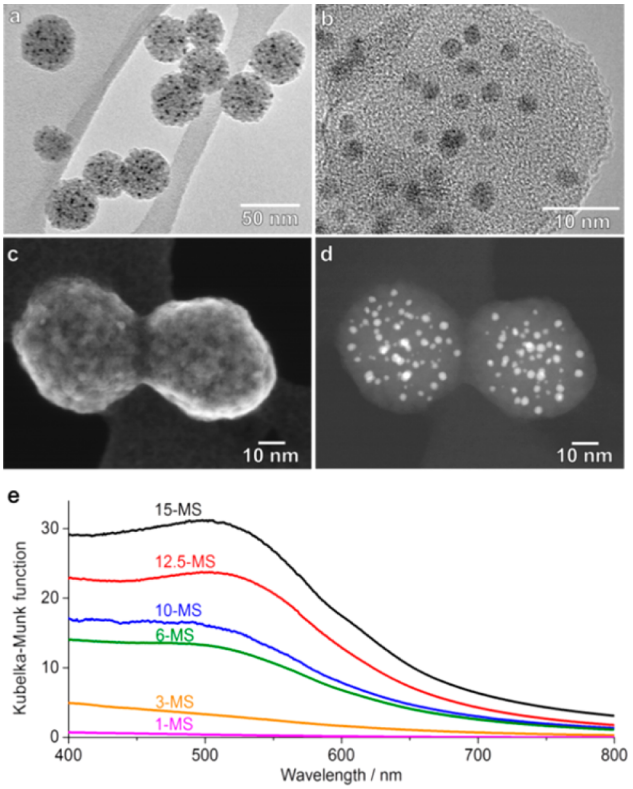

Figure 2. (a, b) Representative TEM (a) and HR-TEM (b) images of 12.5 wt % Au loaded silica spheres (12.5-MS). (c) STEM image of 12.5-MS in secondary electron contrast mode. (d) STEM image in z-contrast of the same particles as in c. (e) Diffuse reflectance UV-vis spectra of Au loaded MS.

In contrast, the Au loaded ordered mesoporous silica materials—having significantly larger Au particles—only show a slightly increased glycerol conversion under illumination, indicating that direct plasmonic photocatalysis is more dominant for smaller Au particles. Thus, mesoporous silica spheres provide a much better platform for deposition of plasmonic Au nanoparticles with smaller particle size.

Since the Au loaded mesoporous silica spheres possessed the best Au particle morphology and consequently the best photocatalytic performance, further experiments were conducted with a series of MS with Au loadings of 1, 3, 6, 10, 12.5, and 15 wt % in order to evaluate the effects of Au loading and particle size on the catalytic performance of the materials. At a low Au loading of 1 wt % no Au particles could be detected with TEM studies (Supporting Information Figure S2), indicating the presence of very small Au clusters or isolated Au atoms. At 3 wt % Au loading, small Au particles with a mean diameter of ≈ 1 nm could be observed from the TEM survey (Supporting Information Figure S2b). As expected for such small nanoparticles, no visible-light absorption due to LSPR could be determined (Figure 2e). At higher Au loadings (6, 10, 12.5, and 15 wt %), the Kubelka−Munk plots showed visible-light absorption due to LSPR centered at 500 nm. TEM studies also showed a similar mean Au particle diameter of 2 nm between medium Au loadings of 6 wt % and very high loadings of 15 wt % (Figure 2a,b and Supporting Information Figure S2). Comparing scanning transmission electron microscopy (STEM) micrographs of 12.5-MS in secondary electron and z-contrast mode (Figure 2c,d) reveals that (compared to the total number of Au particles) only a few Au particles can be identified at the external surface of the silica spheres, which suggests confinement of the Au particles in the inner pores of mesoporous silica spheres, rather than Au deposition on the external surface. The pore confinement of the monodispersed, mesoporous silica spheres limits the growth of the Au particles even at high loadings of 15 wt %, which provides a clear advantage in comparison to nonporous support materials. This observation may explain the small and constant mean Au particle diameter of 2 nm even at markedly high loadings of 15 wt %.

After structural characterization, the materials were tested for glycerol oxidation in order to evaluate the influence of the loading amount of Au nanoparticles on the catalytic performance. As Figure 3 shows, due to the absence of LSPR at low Au

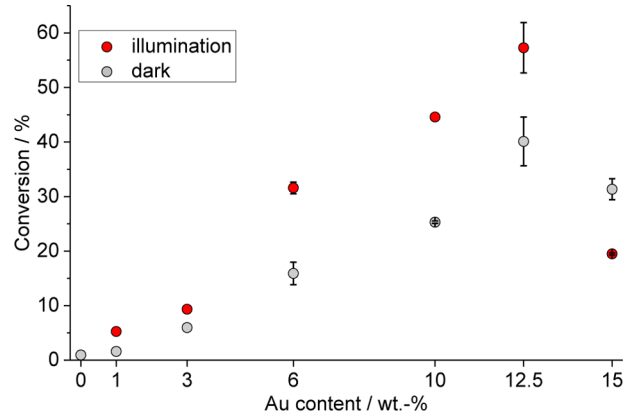

Figure 3. Glycerol conversion of MS loaded with different weight percent Au under visible-light illumination (red dots) and under dark conditions (gray dots).

loadings of 1 and 3 wt %, the glycerol conversion is in good approximation identical with and without visible-light illumination. Under illumination, the glycerol conversion doubles at Au loadings of 6 and 10 wt % and still is considerably higher at an Au loading of 12.5 wt %, where a conversion of around 60% is observed. Further increasing the Au loading to 15 wt % decreases the conversion of the dark and photoassisted reactions, which can be attributed to the pore blocking by Au particles that results in diffusion limitations of the reactants. At a loading of 15 wt %, the photoassisted reaction results in a lower glycerol conversion compared to that of the dark reaction. This can be ascribed to an increase of the gold particle size under visible-light illumination and elevated temperatures.[42] The postreaction TEM survey (Supporting Information Figure S3) indicated that the mean Au particle diameter was increased more strongly under visible-light illumination than under dark reaction conditions, which leads to a lower active surface area and consequentially to a lower glycerol

DOI: 10.1021/acs.chemmater.5b03520
Chem. Mater. 2015, 27, 7743−7750

conversion. The higher conversion under visible-light illumination also leads to changes in the selectivity for product formation (Supporting Information Figure S4). While dihydroxyacetone is the main oxidation product with and without visible-light illumination, the light illumination reduces the dihydroxyacetone selectivity at the expense of higher oxidized products as glyceric acid, glycolic acid, and tartronic acid (Supporting Information Figure S5), which indicates facilitated oxidation of glycerol.

Bimetallic nanoparticles have been shown to result in exceptional catalytic performance in other catalytic reactions due to interfacial and synergistic effects.[43] To further increase the glycerol conversion, a series of bimetallic AuCu NPs with different Au/Cu ratios were supported on (3-aminopropyl)-trimethoxysilane (APS) surface functionalized MS with a constant total metal loading of 6 wt %. The series consists of six samples, of which one was loaded with Au exclusively and one with Cu exclusively to evaluate the effect of AuCu bimetallic particles. APS surface functionalization was employed to ensure homogeneous deposition of the Cu precursor, which was not achieved without surface functionalization as seen in the macroscopic image in Supporting Information Figure S6. The samples are denoted as *X*/*Y*-MS-APS where *X* and *Y* represent the nominal weight percents of Au and Cu, which were confirmed by EDX measurements (Supporting Information Table S2), respectively. After APS functionalization of MS, the mesoporosity of the material was preserved. (Figure 4a,b and Supporting Information Figure S7). The deposition of bimetallic NPs on MS-APS results in a bimodal particle size distribution for Au containing samples, which was confirmed by TEM analysis (Supporting Information Figure S8). The small metal particles possess a mean particle diameter of around 1.5 nm (Figure 4a,b and Supporting Information Figure S8) and therefore are smaller than those observed in the monometallic Au-MS series, which is a result of the narrowed pores upon surface functionalization (Supporting Information Figure S7). The larger metal particles have a mean diameter of approximately 40 nm and are located on the external surface of the silica spheres which can be observed from TEM survey. (Supporting Information Figure S8). 0/6-MS-APS, which exclusively contains Cu, did not show metal NPs in the TEM survey.

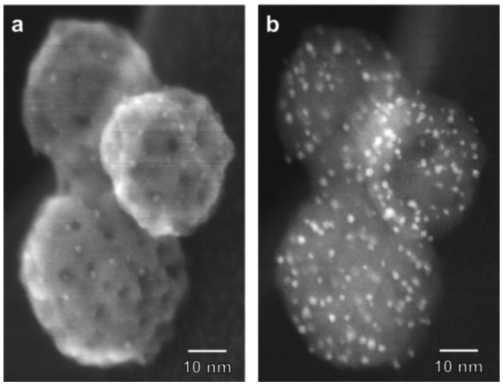

Figure 4. (a) STEM image of 5/1-MS-APS. (b) STEM image in z-contrast of the same particles as in panel a.

In order to identify the oxidation state of copper, the materials were investigated with X-ray photoelectron spectroscopy (XPS). Figure 5 shows the Cu 2p and the Au 4f spectra of 5/1-MS-APS.

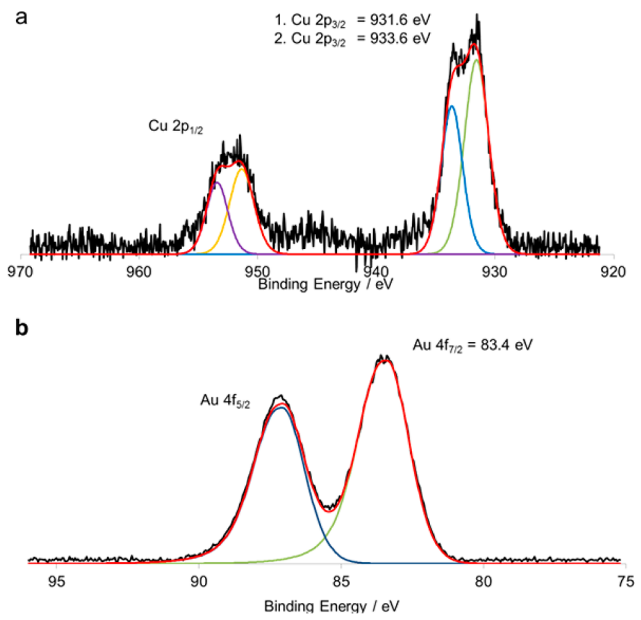

Figure 5. Cu 2p (a) and Au 4f (b) X-ray photoelectron spectra of bimetallic 5/1-MS-APS.

The Cu 2p spectrum shows two Cu $2p_{3/2}$ signals at binding energies of 933.6 and 931.6 eV, respectively, which can be attributed to two different Cu species. As stated in the literature, the distinction between Cu^0 and Cu^I from the Cu $2p_{3/2}$ binding energies alone is not possible.[44] However, the absence of distinct satellite peaks around 945 eV suggests that no Cu^{II} is present in the sample. Thus, it is reasonable to conclude that the two Cu species found by XPS are Cu^0 and Cu^I. The presence of metallic Cu confirms the formation of AuCu alloy. Due to low signal intensity the analysis of the Cu Auger lines for an assignment of Cu^0 and Cu^I was not possible. The Au 4f spectrum (Figure 5b) clearly shows the presence of Au^0. EDX spot analysis of 5/1-MS-APS revealed that the large (40 nm) metal particles are monometallic Au particles, whereas Cu and Au can be found throughout the support (Supporting Information Figure S9 and Table S3). Due to the very low particle diameter of 1.5 nm and the low concentration in the catalyst, powder X-ray diffraction did not yield further evidence for the bimetallic nature of the NPs (data not shown). However, elemental mapping of Au and Cu performed on a Hitachi HD-2700 FE-STEM shows that the spatial distribution of Cu in 5/1-MS-APS matches well with the spatial distribution of Au (Supporting Information Figure S10).

The presence of large Au particles leads to strong visible-light absorption due to LSPR centered at 506 nm (Figure 6a) and thus causes a high concentration of energetic charge carriers under visible-light illumination. However, the large particles only provide a relatively small surface area and possess a significantly lower turnover frequency in selective glycerol oxidation than small Au NPs.[45]

In contrast, the mean particle diameter of 1.5 nm in the small metal particles only allows for minor visible-light absorption but provides a large surface area. Thus, due to the strong visible-light absorption of the large monometallic Au particles, the expected bathochromic shift in absorption, caused by alloying

DOI: 10.1021/acs.chemmater.5b03520
Chem. Mater. 2015, 27, 7743−7750

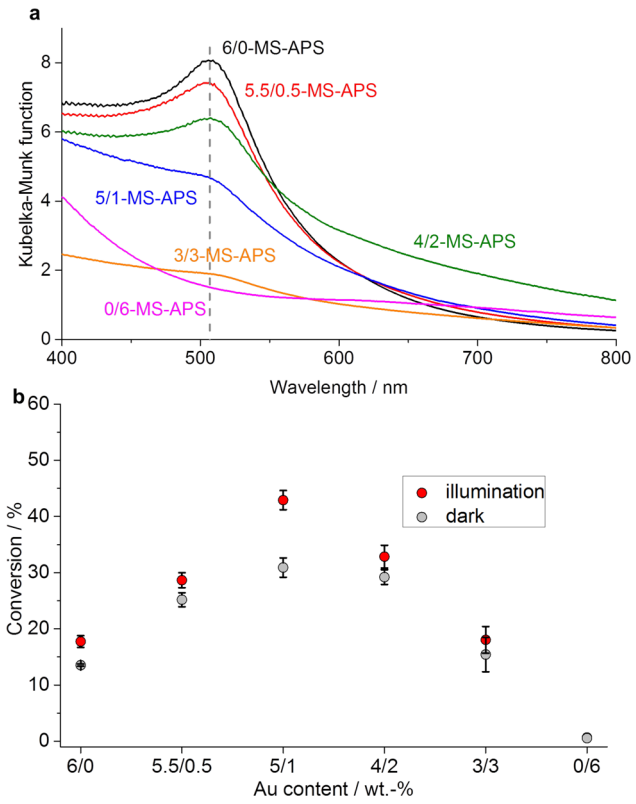

Figure 6. (a) Diffuse reflectance UV-vis spectra of Au/Cu-MS-APS. The gray line shows the absorption maximum of 6/0-MS-APS (506 nm). (b) Glycerol conversion of AuCu-MS-APS.

of Au with Cu, cannot be observed from the diffuse reflectance UV−vis spectra (Figure 6a). However, based on the adopted methodology for the preparation of AuCu bimetallic particle,[46] and our EDX and XPS analyses, we could indirectly corroborate the formation of AuCu alloy nanoparticles.

Comparing the glycerol conversion of both monometallic Au catalysts, namely, 6-MS (Figure 1) and 6/0-MS-APS (Figure 6 b), shows that the photocatalytic rate enhancement is much lower for the APS surface functionalized sample, which can be attributed to the bimodal Au particle size distribution that results in less efficient DPP. Despite the unfavorable particle size distribution, enhanced glycerol conversion can be observed under visible-light illumination (Figure 6b). Compared to the monometallic 6/0-MS-APS, addition of Cu increases the glycerol conversion by a factor of 2.5 at Au and Cu loadings of 5 and 1 wt %, respectively (Figure 6b). At higher Cu loadings, the glycerol conversion decreases and is almost zero when no Au is present (0/6-MS-APS). Thus, the increased (photo-)catalytic performance of the bimetallic Au/Cu catalysts can be ascribed to synergistic effects between Au and Cu. The selectivity toward DHA follows the same trend as the glycerol conversion and is, in the case of 5/1-MS-APS, improved from 80% to 90% compared to 6/0-MS-APS (Supporting Information Figure S11).

CONCLUSION

Conclusively, we have demonstrated that it is possible to enhance the catalytic activity of Au nanoparticles deposited on mesoporous SiO_2 for glycerol oxidation by visible-light-triggered direct plasmonic photocatalysis. Compared to other mesoporous supports, the small domains of monodispersed mesoporous silica spheres lead to a homogeneous deposition of Au NPs inside the support's pores. The cage-like spherical pores of this support stabilize the Au nanoparticles more efficiently than the tubular and interconnected pores of ordered mesoporous silica materials as KIT-6, SBA-15, and MCM-41, which results in small Au nanoparticles with a constant mean diameter of 2 nm for Au loadings between 6 and 15 wt %. The Au diameter is sufficiently large to allow visible-light absorption by localized surface plasmon resonance and, at the same time, provides a large catalytically active surface area. Increased glycerol conversion under visible-light illumination was also found for a series of bimetallic AuCu particles deposited on surface functionalized mesoporous silica spheres. Due to the synergistic effects between Au and Cu, the glycerol conversion was increased by a factor of 2.5, while the selectivity toward the high value fine chemical dihydroxyacetone was improved from 80% to 90%. The concept and materials developed here can also be applied to other traditional catalytic reactions.

ASSOCIATED CONTENT

Supporting Information

The Supporting Information is available free of charge on the ACS Publications website at DOI: 10.1021/acs.chemmater.5b03520.

Detailed calculation for glycerol conversion, selectivity, carbon balance, and errors, EDX measurements, TEM micrographs of Au loaded silica supports and of bimetallic Au/Cu loaded (3-aminopropyl)-trimethoxysilane surface functionalized monodispersed mesoporous silica spheres, Au particle size distribution of 15-MS after glycerol oxidation with and without light, selectivities and carbon balances, chemical structures of oxidation products, macroscopic image of nonsurface functionalized MS after Cu deposition, elemental mapping of Au and Cu of 5/1-MS-APS, pore size distribution and accumulated pore volume of MS and MS-APS from N_2 physisorption, and EDX spot analyses of 5/1-MS-APS (PDF)

AUTHOR INFORMATION

Corresponding Author

*E-mail: tueysuez@kofo.mpg.de.

Notes

The authors declare no competing financial interest.

ACKNOWLEDGMENTS

This work was supported by MAXNET Energy consortium of the Max Planck Society and the Cluster of Excellence RESOLV (EXC 1069) funded by the Deutsche Forschungsgemeinschaft (DFG). We thank H. Bongard and B. Spliethoff for electron microscope analyses (HR-TEM, STEM, and element mapping), S. Palm for EDX analyses, Dr. Claudia Weidenthaler for XPS measurements, and Prof. Candace Chan (Arizona State University) for fruitful discussion.

REFERENCES

(1) Behr, A.; Eilting, J.; Irawadi, K.; Leschinski, J.; Lindner, F. Improved Utilisation of Renewable Resources: New Important Derivatives of Glycerol. *Green Chem.* **2008**, *10*, 13−30.

(2) Besson, M.; Gallezot, P.; Pinel, C. Conversion of Biomass into Chemicals over Metal Catalysts. *Chem. Rev.* **2014**, *114*, 1827−1870.

DOI: 10.1021/acs.chemmater.5b03520
Chem. Mater. 2015, 27, 7743−7750

(3) Zhou, C.-H.; Beltramini, J. N.; Fan, Y.-X.; Lu, G. Q. Chemoselective Catalytic Conversion of Glycerol as a Biorenewable Source to Valuable Commodity Chemicals. *Chem. Soc. Rev.* **2008**, *37*, 527−549.
(4) Liu, Y.; Tuysuz, H.; Jia, C. J.; Schwickardi, M.; Rinaldi, R.; Lu, A. H.; Schmidt, W.; Schuth, F. From Glycerol to Allyl Alcohol: Iron Oxide Catalyzed Dehydration and Consecutive Hydrogen Transfer. *Chem. Commun.* **2010**, *46*, 1238−1240.
(5) Jerome, F.; Pouilloux, Y.; Barrault, J. Rational Design of Solid Catalysts for the Selective Use of Glycerol as a Natural Organic Building Block. *ChemSusChem* **2008**, *1*, 586−613.
(6) Ruppert, A. M.; Weinberg, K.; Palkovits, R. Hydrogenolysis Goes Bio: From Carbohydrates and Sugar Alcohols to Platform Chemicals. *Angew. Chem., Int. Ed.* **2012**, *51*, 2564−2601.
(7) Ketchie, W. C.; Murayama, M.; Davis, R. J. Selective Oxidation of Glycerol over Carbon-Supported AuPd Catalysts. *J. Catal.* **2007**, *250*, 264−273.
(8) Villa, A.; Veith, G. M.; Prati, L. Selective Oxidation of Glycerol under Acidic Conditions Using Gold Catalysts. *Angew. Chem., Int. Ed.* **2010**, *49*, 4499−4502.
(9) Kondrat, S. A.; Miedziak, P. J.; Douthwaite, M.; Brett, G. L.; Davies, T. E.; Morgan, D. J.; Edwards, J. K.; Knight, D. W.; Kiely, C. J.; Taylor, S. H.; Hutchings, G. J. Base-Free Oxidation of Glycerol Using Titania-Supported Trimetallic Au-Pd-Pt Nanoparticles. *ChemSusChem* **2014**, *7*, 1326−1334.
(10) Deng, X.; Dodekatos, G.; Pupovac, K.; Weidenthaler, C.; Schmidt, W. N.; Schüth, F.; Tüysüz, H. Pseudomorphic Generation of Supported Catalysts for Glycerol Oxidation. *ChemCatChem* **2015**, DOI: 10.1002/cctc.201500703.
(11) Prati, L.; Rossi, M. Gold on Carbon as a New Catalyst for Selective Liquid Phase Oxidation of Diols. *J. Catal.* **1998**, *176*, 552−560.
(12) Sugano, Y.; Shiraishi, Y.; Tsukamoto, D.; Ichikawa, S.; Tanaka, S.; Hirai, T. Supported Au-Cu Bimetallic Alloy Nanoparticles: An Aerobic Oxidation Catalyst with Regenerable Activity by Visible-Light Irradiation. *Angew. Chem., Int. Ed.* **2013**, *52*, 5295−5299.
(13) Ryabenkova, Y.; Miedziak, P. J.; Knight, D. W.; Taylor, S. H.; Hutchings, G. J. Heterogeneously catalyzed oxidation of butanediols in base free aqueous media. *Tetrahedron* **2014**, *70*, 6055−6058.
(14) Hoffmann, M. R.; Martin, S. T.; Choi, W. Y.; Bahnemann, D. W. Environmental Applications of Semiconductor Photocatalysis. *Chem. Rev.* **1995**, *95*, 69−96.
(15) Linsebigler, A. L.; Lu, G. Q.; Yates, J. T. Photocatalysis on TiO_2 Surfaces - Principles, Mechanisms, and Selected Results. *Chem. Rev.* **1995**, *95*, 735−758.
(16) Linic, S.; Christopher, P.; Ingram, D. B. Plasmonic-Metal Nanostructures for Efficient Conversion of Solar to Chemical Energy. *Nat. Mater.* **2011**, *10*, 911−921.
(17) Kale, M. J.; Avanesian, T.; Christopher, P. Direct Photocatalysis by Plasmonic Nanostructures. *ACS Catal.* **2014**, *4*, 116−128.
(18) Xiao, Q.; Jaatinen, E.; Zhu, H. Direct Photocatalysis for Organic Synthesis by Using Plasmonic-Metal Nanoparticles Irradiated with Visible Light. *Chem. - Asian J.* **2014**, *9*, 3046−3064.
(19) Xiao, M.; Jiang, R.; Wang, F.; Fang, C.; Wang, J.; Yu, J. C. Plasmon-enhanced chemical reactions. *J. Mater. Chem. A* **2013**, *1*, 5790−5805.
(20) Zhang, X.; Ke, X.; Zhu, H. Zeolite-Supported Gold Nanoparticles for Selective Photooxidation of Aromatic Alcohols under Visible-Light Irradiation. *Chem. - Eur. J.* **2012**, *18*, 8048−8056.
(21) Hallett-Tapley, G. L.; Silvero, M. J.; Bueno-Alejo, C. J.; Gonzalez-Bejar, M.; McTiernan, C. D.; Grenier, M.; Netto-Ferreira, J. C.; Scaiano, J. C. Supported Gold Nanoparticles as Efficient Catalysts in the Solvent less Plasmon Mediated Oxidation of sec-Phenethyl and Benzyl Alcohol. *J. Phys. Chem. C* **2013**, *117*, 12279−12288.
(22) Della Pina, C.; Falletta, E.; Rossi, M. Highly selective oxidation of benzyl alcohol to benzaldehyde catalyzed by bimetallic gold-copper catalyst. *J. Catal.* **2008**, *260*, 384−386.
(23) Ma, C. Y.; Dou, B. J.; Li, J. J.; Cheng, J.; Hu, Q.; Hao, Z. P.; Qiao, S. Z. Catalytic oxidation of benzyl alcohol on Au or Au-Pd nanoparticles confined in mesoporous silica. *Appl. Catal., B* **2009**, *92*, 202−208.
(24) Sugano, Y.; Shiraishi, Y.; Tsukamoto, D.; Ichikawa, S.; Tanaka, S.; Hirai, T. Supported Au-Cu Bimetallic Alloy Nanoparticles: An Aerobic Oxidation Catalyst with Regenerable Activity by Visible-Light Irradiation. *Angew. Chem., Int. Ed.* **2013**, *52*, 5295−5299.
(25) Zhang, K.; Xu, L.-L.; Jiang, J.-G.; Calin, N.; Lam, K.-F.; Zhang, S.-J.; Wu, H.-H.; Wu, G.-D.; Albela, B.; Bonneviot, L.; Wu, P. Facile Large-Scale Synthesis of Monodisperse Mesoporous Silica Nanospheres with Tunable Pore Structure. *J. Am. Chem. Soc.* **2013**, *135*, 2427−2430.
(26) Prieto, G.; Shakeri, M.; de Jong, K. P.; de Jongh, P. E. Quantitative Relationship between Support Porosity and the Stability of Pore-Confined Metal Nanoparticles Studied on $CuZnO/SiO_2$ Methanol Synthesis Catalysts. *ACS Nano* **2014**, *8*, 2522−2531.
(27) Bore, M. T.; Pham, H. N.; Switzer, E. E.; Ward, T. L.; Fukuoka, A.; Datye, A. K. The role of pore size and structure on the thermal stability of gold nanoparticles within mesoporous silica. *J. Phys. Chem. B* **2005**, *109*, 2873−2880.
(28) Minero, C.; Bedini, A.; Maurino, V. Glycerol as a Probe Molecule to Uncover Oxidation Mechanism in Photocatalysis. *Appl. Catal., B* **2012**, *128*, 135−143.
(29) Augugliaro, V.; El Nazer, H. A. H.; Loddo, V.; Mele, A.; Palmisano, G.; Palmisano, L.; Yurdakal, S. Partial Photocatalytic Oxidation of Glycerol in TiO2 Water Suspensions. *Catal. Today* **2010**, *151*, 21−28.
(30) Zhang, Y.; Zhang, N.; Tang, Z.-R.; Xu, Y.-J. Identification of Bi2WO6 as a highly selective visible-light photocatalyst toward oxidation of glycerol to dihydroxyacetone in water. *Chem. Sci.* **2013**, *4*, 1820−1824.
(31) Zhang, K.; Xu, L.-L.; Jiang, J.-G.; Calin, N.; Lam, K.-F.; Zhang, S.-J.; Wu, H.-H.; Wu, G.-D.; Albela, B.; Bonneviot, L.; Wu, P. Facile Large-Scale Synthesis of Monodisperse Mesoporous Silica Nanospheres with Tunable Pore Structure. *J. Am. Chem. Soc.* **2013**, *135*, 2427−2430.
(32) Gabaldon, J. P.; Bore, M.; Datye, A. K. Mesoporous silica supports for improved thermal stability in supported Au catalysts. *Top. Catal.* **2007**, *44*, 253−262.
(33) Kleitz, F.; Choi, S. H.; Ryoo, R. Cubic *Ia3d* Large Mesoporous Silica: Synthesis and Replication to Platinum Nanowires, Carbon Nanorods and Carbon Nanotubes. *Chem. Commun.* **2003**, 2136−2137.
(34) Choi, M.; Heo, W.; Kleitz, F.; Ryoo, R. Facile synthesis of high quality mesoporous SBA-15 with enhanced control of the porous network connectivity and wall thickness. *Chem. Commun.* **2003**, 1340−1341.
(35) Cai, Q.; Lin, W. Y.; Xiao, F. S.; Pang, W. Q.; Chen, X. H.; Zou, B. S. The preparation of highly ordered MCM-41 with extremely low surfactant concentration. *Microporous Mesoporous Mater.* **1999**, *32*, 1−15.
(36) Zanella, R.; Sandoval, A.; Santiago, P.; Basiuk, V. A.; Saniger, J. M. New Preparation Method of Gold Nanoparticles on SiO_2. *J. Phys. Chem. B* **2006**, *110*, 8559−8565.
(37) Awazu, K.; Fujimaki, M.; Rockstuhl, C.; Tominaga, J.; Murakami, H.; Ohki, Y.; Yoshida, N.; Watanabe, T. A Plasmonic Photocatalyst Consisting of Silver Nanoparticles Embedded in Titanium Dioxide. *J. Am. Chem. Soc.* **2008**, *130*, 1676−1680.
(38) Zhu, H. G.; Liang, C. D.; Yan, W. F.; Overbury, S. H.; Dai, S. Preparation of highly active silica-supported Au catalysts for CO oxidation by a solution-based technique. *J. Phys. Chem. B* **2006**, *110*, 10842−10848.
(39) Yamada, K.; Miyajima, K.; Mafune, F. Thermionic Emission of Electrons from Gold Nanoparticles by Nanosecond Pulse-Laser Excitation of Interband. *J. Phys. Chem. C* **2007**, *111*, 11246−11251.
(40) Wang, C.; Astruc, D. Nanogold plasmonic photocatalysis for organic synthesis and clean energy conversion. *Chem. Soc. Rev.* **2014**, *43*, 7188−7216.
(41) Gutierrez, L.-F.; Hamoudi, S.; Belkacemi, K. Synthesis of Gold Catalysts Supported on Mesoporous Silica Materials: Recent Developments. *Catalysts* **2011**, *1*, 97−154.

DOI: 10.1021/acs.chemmater.5b03520
Chem. Mater. 2015, 27, 7743−7750

(42) Zanella, R.; Louis, C. Influence of the Conditions of Thermal Treatments and of Storage on the Size of the Gold Particles in Au/TiO_2 Samples. *Catal. Today* **2005**, *107−108*, 768−777.
(43) Wu, C.-Y.; Lee, Y.-L.; Lo, Y.-S.; Lin, C.-J.; Wu, C.-H. Thickness-Dependent Photocatalytic Performance of Nanocrystalline TiO_2 Thin Films Prepared by Sol-Gel Spin Coating. *Appl. Surf. Sci.* **2013**, *280*, 737−744.
(44) Delannoy, L.; Thrimurthulu, G.; Reddy, P. S.; Methivier, C.; Nelayah, J.; Reddy, B. M.; Ricolleau, C.; Louis, C. Selective hydrogenation of butadiene over TiO_2 supported copper, gold and gold-copper catalysts prepared by deposition-precipitation. *Phys. Chem. Chem. Phys.* **2014**, *16*, 26514−26527.
(45) Ketchie, W. C.; Fang, Y.-L.; Wong, M. S.; Murayama, M.; Davis, R. J. Influence of Gold Particle Size on the Aqueous-Phase Oxidation of Carbon Monoxide and Glycerol. *J. Catal.* **2007**, *250*, 94−101.
(46) Li, L.; Wang, C.; Ma, X.; Yang, Z.; Lu, X. An Au-Cu Bimetal Catalyst Supported on Mesoporous TiO_2 with Stable Catalytic Performance in CO Oxidation. *Chin. J. Catal.* **2012**, *33*, 1778−1782.

DOI: 10.1021/acs.chemmater.5b03520
Chem. Mater. 2015, 27, 7743−7750